Spatial local neighborhood index in hyperspectral remote sensing image

LUO Wenfei[1], **ZHONG Liang**[2]

1. *School of Geographical Science*, *South China Normal University*, *Guangdong Guangzhou* 510631, *China*;
2. *Institute of Remote Sensing Applications*, *Chinese Academy of Sciences*, *Beijing* 100101, *China*

Abstract: Hyperspectral remote sensing image provides not only abundant spectral information but also spatial detailed information. For making full use of the information, this paper considered the variations of the spectral feature among pixels in local neighborhood and researched on a kind of Local Neighborhood Spectral Similarity Measure Index to extract the spatial detailed information. Furthermore, the spectral feature of endmember in local neighborhood was also considered. And a kind of Local Neighborhood Independent Endmember Index was proposed. In experiments, these local neighborhood indexes demonstrated excellent performance in the real hyperspectral image. Based on these work, it can further improve the capability of hyperspectral target detection and identification by combining with spatial and spectral information.

Key words: hyperspectral remote sensing, spectral similarity measure, endmember, local neighborhood index

CLC number: TP751.1 **Document code:** A

Citation format: Luo W F and Zhong L. 2010. Spatial local neighborhood index in hyperspectral remote sensing image. *Journal of Remote Sensing*. **14**(4): 751—760

1 INTRODUCTION

Hyperspectral remote sensing stresses on the distinguishable spectral features of the substances. It relies on its abundant spectral resolution to differentiate the substances by their diagnostic spectral features (Tong *et al*, 2006). In application, hyperspectral remote sensing image also provides important spatial information. The interested targets may exist in the image with very low probability, but they can also occupy single cells with high probability, or be interfered by the background with the same spectral feature but different geometric feature. These embarrass the application of hyperspectral remote sensing analysis techniques, such as anomaly detection. In this case, the capability of target detection and recognition can be greatly improved when combining the spatial and the spectral features of the targets.

The spatial information includes edge contour, texture, and targets that occupy a whole pixel or are embed as sub-pixel. This paper does not consider the texture information. The spatial information gives rise to the significant variations between the pixels in the image. The local neighborhood method, whose application has widely covered image restoration, image segment and many other fields (Kenneth, 2002), is a well-known technique for spatial information extraction in grad image analysis. However, this is not the case in hyperspectral remote sensing image, since the significant variations are the spectral feature not the grad. In this case, Kanade and Shafer (1987) detect the edges in each channel independently and then combine the results by 1-norm, 2-norm or maximal-norm. Verzakov *et al.* (2006) reduces the spectral dimension of the hyperspectral remote sensing image in order to satisfy the requirement of the small number of the samples. And the multivariate techniques, such as Joint Probability Density Functions of Neighbouring Pixels and Conditional Probability Density Functions of Neighboring Pixels Difference, are used to retrieve the spatial information. Gong and Bi (2007) uses linear spectral unmixing technique and then detects the edges from the abundance results of unmixing. The latter two methods provide better improvement on spatial information extraction for hyperspectral remote sensing image.

However, in the procedure of dimension reduction or linear spectral unmixing, especially when a great amount of spectral channels are reduced, the image information will be lost. And the spectral unmixing error will be introduced in to the abundance results. These factors have impacts on the accuracy of the following analysis. Therefore, this paper considers the spatial information extraction from the original spectral dimension of the hyperspectral remote sensing image.

In this case, Bakker and Schmidt (2002) introduce commonly used measures including Euclidean distance, spectral angle distance and intensity difference into weighted Laplace

Received: 2009-07-08; **Accepted**: 2009-08-29

Foundation: Chinese National "863" Programs for High Technology Research and Development (No.2008AA12Z113); Key Project of Chinese National "973" Programs for Fundamental Research and Development (No.2009CB723902) and National Natural Science Foundation of China (No.40901232/D010702, No. 40901225/D010702).

First author biography: LUO Wen-fei (1979—), male, lecturer. He received the Ph.D degrees in the Institute of Remote Sensing Applications, Chinese Academy of Sciences. His research interest include remote sensing image processing and hyperspectral remote sensing. E-mail: luowenfei@irsa.ac.cn

operator. It presents excellent results in extraction of homogeneous surface cover types. Take the case of this technique, this paper first introduces spatial function of spectral measures in Local Neighborhood and discusses a kind of Local Neighborhood Spectral Similarity Measure-Index in more general sense. Further, considering the Linear Mixture Model (LMM) of hyperspectral remote sensing image, the variations between the spectral feature of endmember and background in local neighborhood are introduced into the definition of spatial information and a kind of Local Neighborhood Independent Endmember-Index is proposed.

2 LOCAL NEIGHBORHOOD SPECTRAL SIMILARITY MEASURE INDEX

Local Neighborhood Spectral Similarity Measure Index (LNSSM-Index) focuses on the spectral measures. Spectral measures or spectral similarity measures are used to determine the similarity of two spectra, and also to measure the variations between the spectra.

Let $\boldsymbol{r}_i=(r_{i1}, r_{i2},\cdots, r_{iL})^{\mathrm{T}}$ be a spectral signature of a pixel in the hyperspectral remote sensing image and L be the number of bands.

Spectral Distance Measure (*SDM*) calculates the distance between two spectra, namely p-norm of spectral vectors (Bourbaki, 1987) where

1-norm distance (or Taxicab Distance, *TD*)

$$TD(\boldsymbol{r}_i,\boldsymbol{r}_j)=\sum_{b=1}^{L}\left|r_{ib}-r_{jb}\right| \tag{1}$$

2-norm distance (Euclidean Distance, *ED*)

$$ED(\boldsymbol{r}_i,\boldsymbol{r}_j)=\sqrt{(\boldsymbol{r}_i-\boldsymbol{r}_j)^{\mathrm{T}}(\boldsymbol{r}_i-\boldsymbol{r}_j)} \tag{2}$$

maximum-norm distance (Maximum Distance, *MD*)

$$MD(\boldsymbol{r}_i,\boldsymbol{r}_j)=\max_{1\leqslant b\leqslant L}\left\{\left|r_{ib}-r_{jb}\right|\right\} \tag{3}$$

Another spectral measure called Spectral Angle Measure (*SAM*) calculates the vectors' angle between two spectral (Robert, 2006)

$$SAM(\boldsymbol{r}_i,\boldsymbol{r}_j)=\cos^{-1}\left(\boldsymbol{r}_i^{\mathrm{T}}\boldsymbol{r}_j/\left\|\boldsymbol{r}_i\right\|\left\|\boldsymbol{r}_j\right\|\right) \tag{4}$$

And Spectral Information Divergence (*SID*) measures the discrepancy between two spectral signature-derived probability distributions (Chang, 2000)

$$SID(\boldsymbol{r}_i,\boldsymbol{r}_j)=D(\boldsymbol{r}_i\,\|\,\boldsymbol{r}_j)+D(\boldsymbol{r}_j\,\|\,\boldsymbol{r}_i) \tag{5}$$

where

$$D(\boldsymbol{r}_i\,\|\,\boldsymbol{r}_j)=\sum_{b=1}^{L}q_b log\left(\frac{q_b}{p_b}\right) \tag{6}$$

and

$$q_b=r_{ib}\Big/\sum_{l=1}^{L}r_{il} \tag{7}$$

$$p_b=r_{jb}\Big/\sum_{l=1}^{L}r_{jl} \tag{8}$$

Define $SSM(\boldsymbol{r}_i, \boldsymbol{r}_j)$ as a function of spectral measure, where the smaller absolute value represents that the spectral signatures are more similar, and vice versa. Specially, the value should be or approach zero when the spectral signatures are the same. Usually, it can simply take polynomial *SDM*, *SAM* or *SID* as *SSM*. When it combines with more spectral measures such as *SID* and *SAM* (Du *et al.*, 2003) into LNSSM-Index, it should be satisfied with the *SSM*.

The value of spectral measures varies with the spatial location of the pixel in the image, which presents a spatial function of spectral measures. Based on *SSM*, spatial function of spectral measures presents the spectral variations in the local neighborhood and extracts the spatial information of the image.

For example, in traditional edge detection technique, the gray gradient represents the gray variations in the horizontal or the vertical direction as follows

$$\boldsymbol{\Delta}_{\mathrm{x}}=\begin{bmatrix}-1 & 0 & 1\\ -a & 0 & a\\ -1 & 0 & 1\end{bmatrix} \tag{9}$$

$$\boldsymbol{\Delta}_{\mathrm{y}}=\begin{bmatrix}-1 & -a & -1\\ 0 & 0 & 0\\ 1 & a & 1\end{bmatrix} \tag{10}$$

where a is 1 or 2, corresponding to Prewitt or Sobel edge operators respectively. In hyperspectral remote sensing image, the spatial function of spectral measures in the corresponding location represents the spectral variations as follows

$$\begin{aligned}d_{\mathrm{x}}(x,y)=&SSM(\boldsymbol{I}(x+1,y-1),\boldsymbol{I}(x-1,y-1))\\&+a\times SSM(\boldsymbol{I}(x+1,y),\boldsymbol{I}(x-1,y))\\&+SSM(\boldsymbol{I}(x+1,y+1),\boldsymbol{I}(x-1,y+1))\end{aligned} \tag{11}$$

where $\boldsymbol{I}(x, y)$ is the spectral signature located at (x, y). It is similar in the vertical case.

Similarly, in the case of second-order derivation, eight directions Laplace operator follows that

$$d^2(x,y)=\sum_{i=-1}^{1}\sum_{j=-1}^{1}SSM(\boldsymbol{I}(x,y),\boldsymbol{I}(x-i,y-j)) \tag{12}$$

In the case of weighted Laplace operator, it can refer to the work of Bakker and Schmidt (2002).

By spatial function of spectral measures, the spectral variations in the local neighborhood can be determined and the spatial information can be extracted. Nevertheless, LNSSM-Index is not merely limited to edge detection technique. Any spatial functions of spectral measures which express the spectral variations in the local neighborhood can be taken as LNSSM-Index. For example, the spatial function of *SSM* between the mean spectral in the local neighborhood and the spectral at the central location of the local neighborhood, the spatial function of *SSM* between the weighted mean spectral in the local neighborhood and the spectral at the central location of the local neighborhood can be further considered, and so on.

3 LOCAL NEIGHBORHOOD INDEPENDENT ENDMEMBER INDEX

By Linear Mixture Model (LMM), hyperspectral remote sensing image can be modeled as

$$\boldsymbol{r}=\boldsymbol{M}\boldsymbol{a}+\boldsymbol{n} \tag{13}$$

where $\boldsymbol{r}$ is the spectral signature of a pixel in hyperspectral remote sensing image, $\boldsymbol{M}$ is the endmember matrix whose columns are the endmember signature vectors, $\boldsymbol{a}$ is the fractional abundance vector associated with $\boldsymbol{r}$, whose entries are the fractional abundance corresponding to the endmembers in $\boldsymbol{M}$, and $\boldsymbol{n}$ is the additive observation noise vector. According to LMM, the endmembers reside at the extremities of the simplex volume occupied by the image. When the substance in a pixel is differed from those in other pixels (called background) within its local neighborhood, its spectral signature vector is far from the subspace spanned by the spectral signature vectors of background in the spectral feature space. This spectral signature vector is taken as an independent endmember from its local neighborhood background. Obviously, if the independent endmember has the greater purity, the projection distance to the subspace spanned by its local neighborhood background will be farther. Local Neighborhood Independent Endmember Index (LNIE-Index) takes the purity of the independent endmember as a measure for the detailed spatial information.

The first type of LNIE-Index, called Endmember Background Distance Index (*EBDI*), obtains the projection distance from the spectral signature vector in the center of local neighborhood to the subspace spanned by the signature vectors of its local neighborhood background as follows

$$EBDI(x,y)=\left\|\boldsymbol{P}^{\mathrm{T}}\cdot\boldsymbol{I}(x,y)\right\|_2 \tag{14}$$

$$\boldsymbol{P}=\overline{\boldsymbol{A}}^{+}\overline{\boldsymbol{A}} \tag{15}$$

Eq.(14) obtains the subspace projection distance by null space (Luo *et al*., 2008a), where $\boldsymbol{A}$ is the matrix whose columns are the spectral signature vectors of local neighborhood background, $\overline{\boldsymbol{A}}$ is a base of null space determined by $\boldsymbol{A}$ and $\overline{\boldsymbol{A}}^{+}$ is the Moore-Penrose pseudo-inverse of $\overline{\boldsymbol{A}}$.

Another type of LNIE-Index is called Cumulative Distance Index (*CDI*) defined by

$$CDI_i(x,y)=CDI_{i-1}(x,y)+d_i \tag{16}$$

$$CDI_1(x,y)=0 \tag{17}$$

where i is from 2 to the number of the pixels in the local neighborhood and

$$d_i=\max_{\boldsymbol{r}}\left(\left\|\boldsymbol{P}_{i-1}{}^{\mathrm{T}}\cdot\boldsymbol{r}\right\|_2\right) \tag{18}$$

$$\boldsymbol{P}_{i-1}=\overline{\boldsymbol{A}}_{i-1}^{+}\overline{\boldsymbol{A}}_{i-1} \tag{19}$$

$$\boldsymbol{a}_i=\operatorname*{argmax}_{\boldsymbol{r}}\left(\left\|\boldsymbol{P}_{i-1}{}^{\mathrm{T}}\cdot\boldsymbol{r}\right\|_2\right) \tag{20}$$

$$\boldsymbol{A}_i=[\boldsymbol{A}_{i-1},\boldsymbol{a}_i] \tag{21}$$

$$\boldsymbol{A}_1=\boldsymbol{I}(x,y) \tag{22}$$

where $\operatorname*{argmax}_{\boldsymbol{r}}(\bullet)$ is the spectral signature satisfied with the maximum condition, $\boldsymbol{r}$ is arbitrary spectral signature vector in the local neighborhood, $\boldsymbol{A}_i$ is the matrix made up of endmember signature vectors generated in the i-th step, d_i is the maximal projection distance from the subspace spanned by the column vectors of $\boldsymbol{A}_{i-1}$ and $\boldsymbol{a}_i$ is the corresponding spectral signature vector.

CDI cumulates all the maximal projection distances during the iterations. When there exist more cover types in the local neighborhood or the spectral signature in the local neighborhood is more different from others, the *CDI* value is greater. While the cover type in the local neighborhood is more homogeneous, the *CDI* value is less. By *CDI* value, the detail spatial information can be determined.

4 EXPERIMENT

The AVIRIS (Airborne Visible/Infrared Imaging Spectrometer) sensor has 224 channels over the 0.37—2.51μm spectral range with an average spectral resolution of 10 nm. In experiment, we use a 400×400 pixels subimage of the Feb 20, 2002, a naval air station in San Diego, California reflectance data set with spatial resolution of 3.5m (See Fig. 1).

On the left bottom of Fig. 1 is the 3x zoom image for three airplane targets. We first apply RXD-UDT anomaly detector (Chang, 2002) on the image. The result (see Fig.2) shows that the airplanes can hardly be detected.

Fig. 1 AVIRIS data in San Diego (display band: 458nm)

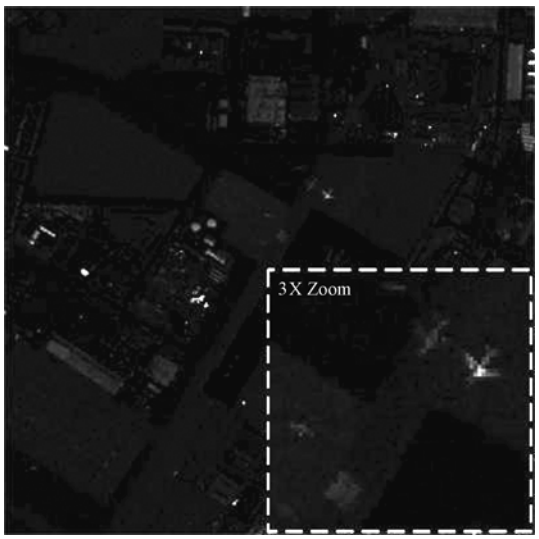

Fig. 2 Result of RXD-UDT anomaly detection

We calculate LNSSM-Indexes and LNIE-Indexes from the image respectively (See Fig.3 and Fig.4). Infinity norm type *SDM-ED*, *SAM-ED* and *SID-EM* are used in LNSSM-Indexes. Sobel and eight direction Laplacian operators are used. *EBDI* and *CDI* are used in LNIE-Indexes.

Comparing the Laplace operator and Sobel operator with different spectral measures in Fig.3, there is different performance on the operators. (1) In *SDM*, Sobel operator extracts the line edges better than Laplace operator while Laplace operator extracts the irregular edges, such as the edges of the building and airplane, better than Sobel operator. (2) In *SAM*, the extracted edges are thinner than that extracted by other spectral measures, but much information is missed, such as the edges of the runways, the flat grounds and the buildings. And more information is missed by Sobel operator than Laplace operator. (3) In *SID*, all the edges are clearly extracted by both Sobel operator and Laplace operator, even the small targets, such as three airplanes in 3x zoom image and the small targets arrayed in the flat ground in the bottom left of the image. However, there exists noise in *SID*, especially in the result of Sobel operator. The noise in the flat ground in up left is much greater than that of Laplace operator.

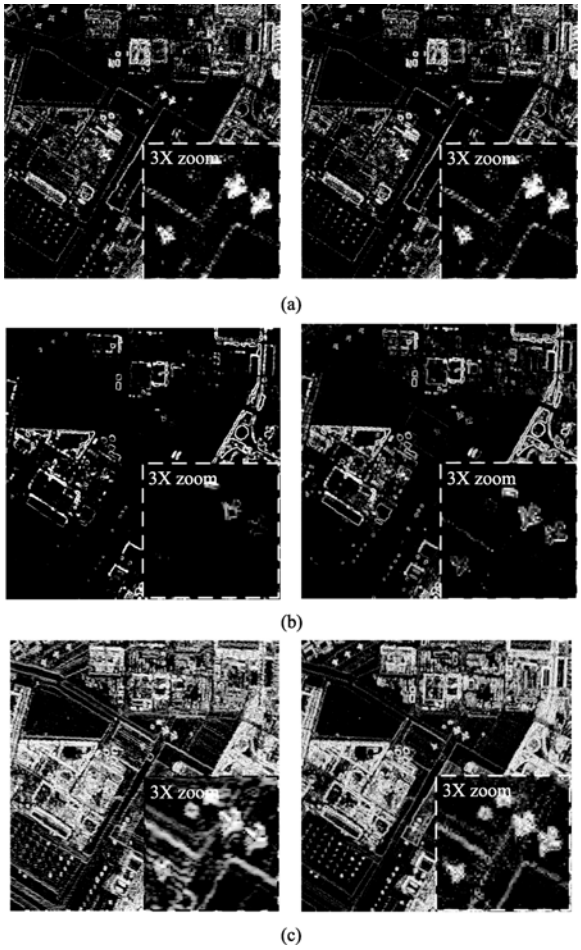

Fig. 3 Results of Local Neighbor Spectral Measure Indexes (Up row: Sobel operator; Down row: Laplace operator)
(a) *SDM* (*MD*); (b) *SAM*; (c) *SID*

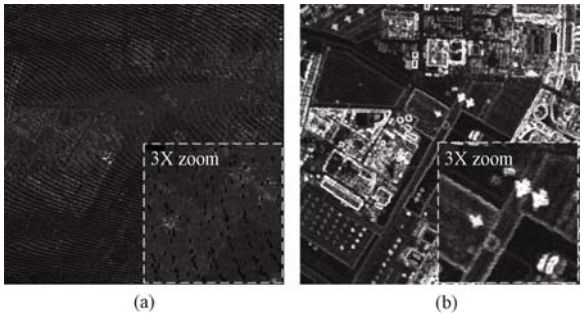

Fig. 4 Results of Local Neighbor Independent Endmember Indexes
(a) *EBDI*; (b) *CDI*

In the results of Local Neighbor Independent Endmember Indexes, all detail spatial information can be clearly extracted by *CDI*, including the edges of flat grounds, the runways, the buildings and the small targets. However, it does not work very well by *EBDI*. The reason is that there is continuity between the ground truths in the scene of the image and the spectral signature in the center of the local neighborhood is easily embedded in the subspace spanned by the background spectral signature vectors. While *CDI* cumulates all the maximal projection distances during the iterations, a part of similar spectral signatures does not have a great effect on *CDI*. Therefore, *CDI* effectively avoids the interfering made by the similar spectral signatures in the local neighborhood.

5 CONCLUSIONS

This paper discusses on two kinds of local neighborhood indexes, namely LNSSM-Index and LNIE-Index, to extract the detailed spatial information from hyperspectral remote sensing image.

In LNSSM-Index, *SDM* can be used to extract the line edges, such as the edges of runways, but does not work well for the small targets extraction. The edges extracted by *SAM* are thinner than other spectral measures. But it is not suggested using *SAM* to extract the line edges and the edges of a large region. *SID* can be used to extract the small targets and the line edges. But *SID* is easily interfered by the noise. When there is much noise in the image, it is strongly suggested removing the noise before using *SID*.

In LNIE-Index, *EBDI* is easily interfered by the similar spectral signatures in the local neighborhood. Therefore, the objects which have spatial continuity, including the line and region continuity and the targets whose radiative region exceeds a pixel of the image, can not be extracted by *EBDI*. *CDI* has the best performance for the line edges such as runways, the edges of a large region such as flat ground and irregular edges such as buildings. Therefore, *CDI* is suitable to extract all the detailed spatial information.

Our future work will be: (1) to verify the indexes proposed in this paper with different levels of spatial resolution; (2) to introduce more suitable spatial function of spectral measures

and develop more effective local neighborhood indexes; (3) to combine the geometric feature and the spectral feature of the targets to improve the accuracy of target detection and recognition, this is the work we will focus on.

Acknowledgements: The authors acknowledge JPL (Jet Propulsion Laboratory) and ENVI (The Environment for Visualizing Images, copyright by ITT Corporation) for providing AVIRIS data.

REFERENCES

Bakker W H and Schmidt K S. 2002. Hyperspectral edge filtering for measuring homogeneity of surface cover types. *Journal of Photogrammetry & Remote Sensing*, 2002, **56**: 246—256

Bourbaki N. 1987. Topological Vector Spaces, Chapters 1—5: Elements of Mathematics. Berlin: Springer-Verlag

Chang C I. 2002. Hyperspectral Imageing Techniques for Spectral Detection and Classification. New York: Kluwer Academic/ Plenum Publishers

Chang C I. 2000. An information theoretic-based approach to spectral variability, similarity and discriminability for hyperspectral image analysis. *IEEE Transation on Information Theory*, **46**(5): 1927—1932

Du Y, Chang C I, Ren H, Amico F D and Jensen J O. 2003. A new hyperspectral discrimination measure for spectral similarity. Algorithms and Technologies for Multispectral, Hyperspectral, and Ultraspectral Imagery IX, SPIE Digital Library

Gong Y and Bi D. 2007. The edge detection of hyperspectral image based on its proportion image. 27th International Congress on High-Speed Photography and Photonics. SPIE Digital Library

Kanade T and Shafer S. 1987. Image understanding research at cmu. Proceedings of an Image Understanding Workshop, Los Angeles, CA:Morgan Kaufmann Publishers

Kenneth R C. 2002. Digital Image Processing 2ed. Beijing: Publishing House of Electronics Industry

Luo W F, Zhong L, Zhang B and Gao L R. 2008. An spectral unmixing algorithm for hyperspectral image based on the distance to subspace. *Progress in Natural Science*, **18**(10):1175—1180

Schowengerdt R A. 2006. Remote Sensing 3ed: Models and Methods for Image Processing. Missouri, USA :Academic Press

Tong Q X, Zhang B and Zheng L F. 2006. Hyperspectral Remote Sensing. Beijing: Higher Education Press

Verzakov S, Paclik P and Duin R P W. 2006. Edge detection in hyperspectral imaging: multivariate statistical approaches. Lecture Notes in Computer Science. Berlin:Springer Verlag

高光谱遥感图像的空间邻域指数

罗文斐[1]，钟 亮[2]

1. 华南师范大学 地理科学学院，广东 广州 510631;
2 中国科学院遥感应用研究所，北京 100101

摘 要： 通过高光谱遥感图像空间邻域内光谱特征的变化，研究了邻域光谱度量指数；根据邻域内端元光谱特征的变化，提出了邻域独立端元指数提取图像的空间维细节信息。通过真实高光谱遥感图像检验，两类邻域指数能够较好地提取高光谱遥感图像中的细节，为进一步结合空间维、光谱维特征的高精度目标探测与识别创造了有利条件。

关键词： 高光谱遥感，光谱相似性度量，端元，邻域指数

中图分类号： TP751.1 文献标识码： A

引用格式: 罗文斐，钟 亮. 2010. 高光谱遥感图像的空间邻域指数. 遥感学报, **14**(4): 751—760
Luo W F and Zhong L. 2010. Spatial local neighborhood index in hyperspectral remote sensing image. *Journal of Remote Sensing*. **14**(4): 751—760

1 引 言

高光谱遥感强调地物所特有的光谱特征，凭借足够的光谱分辨率来区分这些具有诊断性光谱特征的地物(童庆禧等，2006)。在实际应用中，高光谱遥感图像提供的空间维信息也同样重要，我们感兴趣的目标地物在图像中可能低概率出现，但也会以单个体的形式频繁地出现，甚至在图像中存在与目标光谱特征一致但几何特征不同的背景地物。各种因素的干扰，导致了高光谱遥感图像分析技术(如异常探测)受到一定的限制。如果能够结合图像中的光谱维特征与空间维特征，将有助于提高对高光谱遥感图像的理解，大大提高对目标地物的探测、识别能力。

图像在空间维上所提供的信息，包括了地物的边缘轮廓、纹理以及点状整像元或亚像元小目标的细节(本文暂不考虑纹理)，这些细节主要通过图像中像元间的差异体现。利用邻域像元提取图像的空间维信息在传统的图像分析中是一项比较成熟的技术，已广泛应用在图像复原、图像分割等各个领域(Kenneth, 2002)。但对于高光谱遥感图像，对像元光谱间差异的描述不同于传统的全色、多光谱遥感图像，它主要强调光谱的差异，而非灰度的差异。这方面的研究，早期 Kanade 和 Shafer(1987)通过独立地对各个波段进行边缘检测，再对每个波段检测的结果采用向量范数进行合并，从而获取图像的边缘信息。但这种方法应用到高光谱遥感图像中的效果并不十分理想, Verzakov 等(2006)先经过图像降维处理，以保证邻域内样本的数量符合维度的要求，通过联合概率密度或条件概率密度获得邻域像元间的差异。Gong 和 Bi(2007)先对高光谱遥感图像进行线性光谱解混，在各丰度图像中分别进行边缘检测，获取不同地物的边缘信息。后两种方法在高光谱遥感图像上有了较好的改进。

然而，大多数方法由于在降维、线性光谱解混的过程中，会损失一部分图像信息(尤其当维度大幅度减少时)，或引入新的误差(如光谱解混的误差)，这将影响后续图像分析的精度。因此，本文考虑直接在图像高维特征空间当中，提取图像空间维的信息，以避免各种处理所造成的影响。

在这一方面，Bakker 和 Schmidt(2002)把常用的欧氏距离、角度度量以及强度差异成功引入到了加权拉普拉斯边缘检测算子当中，并且在同质地表覆盖类型信息的提取中取得了不错的效果。以这一技

收稿日期：2009-07-08；修订日期：2009-08-29

基金项目：国家 863 项目(编号: 2008AA12Z113)；国家 973 项目(编号: 2009CB723902)和国家自然科学基金项目(编号: 40901232/D010702、40901225/D010702)。

第一作者简介：罗文斐(1979—)，男，讲师，2008 年博士毕业于中国科学院遥感应用研究所，目前主要从事遥感图像处理、高光谱遥感方面的研究工作。E-mai: luowenfei@irsa.ac.cn。

术为例，本文首先引入了邻域内光谱度量的空间函数，阐述了一类更具一般意义的邻域光谱度量指数。并进一步从高光谱遥感图像线性混合模型(Linear Mixture Model, LMM)的角度，通过邻域内独立的端元光谱与周围地物光谱间的差异，以达到凸显端元地物的目的，从而提出了邻域独立端元指数。

2 邻域光谱度量指数

光谱度量(又称“光谱相似性度量”)用于衡量待定光谱与参考光谱间的相似性，同样也用于衡量光谱间的差异性。

记 $\boldsymbol{r}_i=(r_{i1}, r_{i2}, \cdots, r_{iL})^{\mathrm{T}}$ 为图像 I 中任意光谱像元，L 为波段数。

光谱距离度量(Spectral Distance Measure, *SDM*)计算了两光谱间的距离，即光谱向量的 p-范数(Bourbaki, 1987):

1-范数的 Taxicab 距离(Taxicab Distance, *TD*)

$$TD(\boldsymbol{r}_i,\boldsymbol{r}_j)=\sum_{b=1}^{L}\left|r_{ib}-r_{jb}\right| \tag{1}$$

2-范数的欧式距离(Euclidean Distance, *ED*)

$$ED(\boldsymbol{r}_i,\boldsymbol{r}_j)=\sqrt{(\boldsymbol{r}_i-\boldsymbol{r}_j)^{\mathrm{T}}(\boldsymbol{r}_i-\boldsymbol{r}_j)} \tag{2}$$

无穷范数的最大距离(Maximum Distance, *MD*)

$$MD(\boldsymbol{r}_i,\boldsymbol{r}_j)=\max_{1\leqslant b\leqslant L}\left\{\left|\boldsymbol{r}_{ib}-\boldsymbol{r}_{jb}\right|\right\} \tag{3}$$

光谱角度度量(Spectral Angle Measure, *SAM*)计算了两光谱之间的角度差异(Robert, 2006):

$$SAM(\boldsymbol{r}_i,\boldsymbol{r}_j)=\cos^{-1}\left(\boldsymbol{r}_i^{\mathrm{T}}\boldsymbol{r}_j/\left\|\boldsymbol{r}_i\right\|\left\|\boldsymbol{r}_j\right\|\right) \tag{4}$$

光谱信息散度(Spectral Information Divergence, *SID*)比较了两光谱的信息散度(Chang, 2000):

$$SID(\boldsymbol{r}_i,\boldsymbol{r}_j)=D(\boldsymbol{r}_i\,\|\,\boldsymbol{r}_j)+D(\boldsymbol{r}_j\,\|\,\boldsymbol{r}_i) \tag{5}$$

其中

$$D(\boldsymbol{r}_i\,\|\,\boldsymbol{r}_j)=\sum_{b=1}^{L}q_b\log\left(\frac{q_b}{p_b}\right) \tag{6}$$

且

$$q_b=r_{ib}\Big/\sum_{l=1}^{L}r_{il} \tag{7}$$

$$p_b=r_{jb}\Big/\sum_{l=1}^{L}r_{jl} \tag{8}$$

令 $SSM(\boldsymbol{r}_i, \boldsymbol{r}_j)$为光谱度量的函数，且函数的绝对值应越小，表示两像元的光谱越相似，反之亦然，特别地，当两光谱完全一致时，其函数值趋向于或等于零。通常，可以简单地把 *SDM*、*SAM* 或 *SID* 的多项式函数作为 *SSM*。当需要混合使用多种光谱度量，例如把 *SID-SAM* 度量(Du 等，2003)应用到邻域光谱指数时，只需判断是否符合 *SSM* 函数。

光谱度量随着图像像元的空间位置不同而发生变化，体现为光谱度量的空间函数。以 *SSM* 为基础，通过光谱度量的空间函数能够表达邻域内光谱特征的变化情况，进而反映图像的空间细节信息。

例如，在传统的边缘检测技术中，图像灰度的梯度反映了水平、垂直方向上像元灰度的差异，其卷积核为:

$$\Delta_{\mathrm{x}\,方向}=\begin{bmatrix}-1 & 0 & 1\\ -a & 0 & a\\ -1 & 0 & 1\end{bmatrix} \tag{9}$$

$$\Delta_{\mathrm{y}\,方向}=\begin{bmatrix}-1 & -a & -1\\ 0 & 0 & 0\\ 1 & a & 1\end{bmatrix} \tag{10}$$

当 a 的值为 1 或 2 时，分别对应了 Prewitt、Sobel 边缘算子。在高光谱遥感图像中，对应位置的 *SSM* 光谱度量空间函数反映了该邻域的光谱差异:

$$\begin{aligned}d_{\mathrm{x}方向}(x,y)=&SSM(\boldsymbol{I}(x+1,y-1),\boldsymbol{I}(x-1,y-1))\\&+a\times SSM(\boldsymbol{I}(x+1,y),\boldsymbol{I}(x-1,y))\\&+SSM(\boldsymbol{I}(x+1,y+1),\boldsymbol{I}(x-1,y+1))\end{aligned} \tag{11}$$

其中，$\boldsymbol{I}(x, y)$表示图像(x, y)位置上的像元光谱。y 方向也作类似的处理。

同样，二阶微分的八方向拉普拉斯边缘算子的光谱度量空间函数表示为:

$$d^2(x,y)=\sum_{i=-1}^{1}\sum_{j=-1}^{1}SSM(\boldsymbol{I}(x,y),\boldsymbol{I}(x-i,y-j)) \tag{12}$$

加权拉普拉斯算子的情况可参考 Bakker 和 Schmidt(2002)的工作。

邻域光谱度量指数强调了通过光谱度量空间函数描述的邻域光谱差异来表达邻域内的空间维细节信息。应该注意，这类指数远不局限于边缘检测技术，能反映邻域内光谱变化的光谱度量空间函数均属于邻域光谱度量指数的范畴，例如，可进一步考虑邻域均值光谱与空间位置在邻域中心的 *SSM* 函数、邻域加权均值光谱与空间位置在邻域中心的 *SSM* 函数等。

3 邻域独立端元指数

高光谱遥感图像可通过线性混合模型进行描述:对于图像中任意像元，有

$$\boldsymbol{r}=\boldsymbol{M}\boldsymbol{a}+\boldsymbol{n} \tag{13}$$

式中，$\boldsymbol{M}$ 为图像的端元矩阵，$\boldsymbol{a}$ 为各端元在像元中的丰度，$\boldsymbol{n}$ 为噪声。在 LMM 下，端元体现为高维单形体的顶点，根据这一特征，在邻域内由于某类地物

的突然出现，将使该地物独立于周围的地物(视作背景)，在光谱特征空间中，将导致该像元光谱远离它在其余像元所张的子空间，此时，该像元在邻域内体现为独立的端元。显然，独立端元光谱的纯度越高，这种差距就会越明显，因此，邻域独立端元指数利用了独立端元光谱的纯度来突出图像的细节。

当以邻域中心像元在光谱特征空间中的位置为固定点，计算它与邻域内其余像元所张子空间的投影距离，即可得到第一类邻域独立端元指数，端元-背景距离指数(Endmember Background Distance Index, *EBDI*):

$$EBDI(x,y)=\left\|\boldsymbol{P}^{\mathrm{T}}\cdot\boldsymbol{I}(x,y)\right\|_2 \tag{14}$$

$$\boldsymbol{P}=\bar{\boldsymbol{A}}^{+}\bar{\boldsymbol{A}} \tag{15}$$

式中，$\boldsymbol{A}$ 为邻域内除了 $\boldsymbol{I}(x, y)$外其余像元光谱所组成的列向量矩阵，$\bar{\boldsymbol{A}}$表示 $\boldsymbol{A}$ 零空间的一个基，$\bar{\boldsymbol{A}}^{+}$表示 $\bar{\boldsymbol{A}}$的 Moore-Penrose 广义逆矩阵。式(14)通过零空间计算了邻域中心像元与其他像元所张子空间的距离(罗文斐等, 2008)。

累计距离指数(Cumulative Distance Index, *CDI*)则是另一类邻域独立端元指数:

$$CDI_i(x,y)=CDI_{i-1}(x,y)+d_i \tag{16}$$

$$CDI_1(x,y)=0 \tag{17}$$

i 从 2 开始按式(16)的方式递增，直到达到邻域内像元的个数结束，其中

$$d_i=\max_{\boldsymbol{r}}\left(\left\|\boldsymbol{P}_{i-1}{}^{\mathrm{T}}\cdot\boldsymbol{r}\right\|_2\right) \tag{18}$$

$$\boldsymbol{P}_{i-1}=\bar{\boldsymbol{A}}_{i-1}^{+}\bar{\boldsymbol{A}}_{i-1} \tag{19}$$

$$\boldsymbol{a}_i=\operatorname*{argmax}_{\boldsymbol{r}}\left(\left\|\boldsymbol{P}_{i-1}{}^{\mathrm{T}}\cdot\boldsymbol{r}\right\|_2\right) \tag{20}$$

$$\boldsymbol{A}_i=[\boldsymbol{A}_{i-1},\boldsymbol{a}_i] \tag{21}$$

$$\boldsymbol{A}_1=\boldsymbol{I}(x,y) \tag{22}$$

$\operatorname*{argmax}_{\boldsymbol{r}}(\bullet)$ 表示取达到最大值条件的那个光谱向量，$\boldsymbol{r}$ 表示取邻域内的任意像元。式(19)的含义与式(15)相同，其中，$\boldsymbol{A}_i$ 的含义为当前已选取的 i 个像元光谱组成列光谱向量矩阵，在邻域中计算与 $\boldsymbol{A}_{i-1}$ 所张子空间最大光谱投影距离 d_i，并选取具有最大距离的像元 $\boldsymbol{a}_i$ 作为新选择的光谱向量。可见，式(16)累计了整个迭代过程中的最大距离。

由 *CDI* 的定义容易看出，*CDI* 综合考虑了邻域内所有像元的端元光谱投影距离变化情况。当邻域内地物类型越多、光谱差异越大，则 *CDI* 越大。相反，如果邻域内地物均匀单一，则 *CDI* 越小，从而突出了图像的细节。

4 实 验

实验采用了加利福尼亚州-圣地亚哥地区某海军机场的 AVIRIS(Airborne Visible/Infrared Imaging Spectrometer)航空高光谱数据(400×400 像元，空间分辨率 3.5m, 2002-02-20 飞行)，实验中选择了 429—2470nm 的 189 个波段(去除了大气吸收波段)，并经过辐射定标、几何校正、大气校正后，对反射率图像进行算法检验，如图 1。

图 1 中有多架飞机，其中 3 架飞机被放大了 3 倍放于图像的右下角。首先使用 RXD-UDT 异常目标探测算子(Chang, 2002)对图像进行异常目标探测，如图 2，结果表明，异常目标探测技术难以自动分辨出飞机目标。

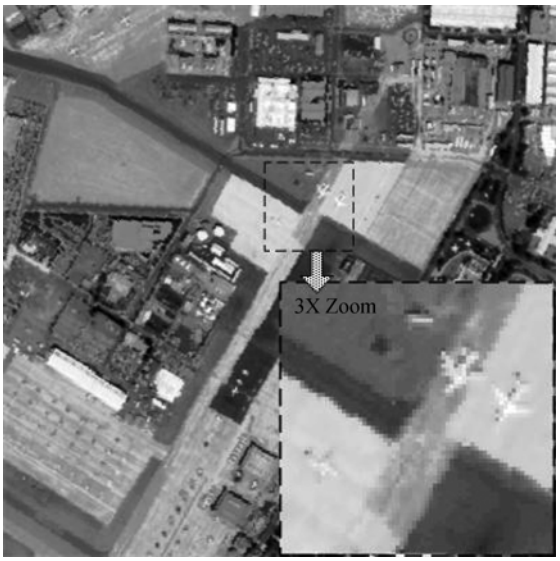

图 1 圣地亚哥地区 AVIRIS 图像(显示波段: 458nm)

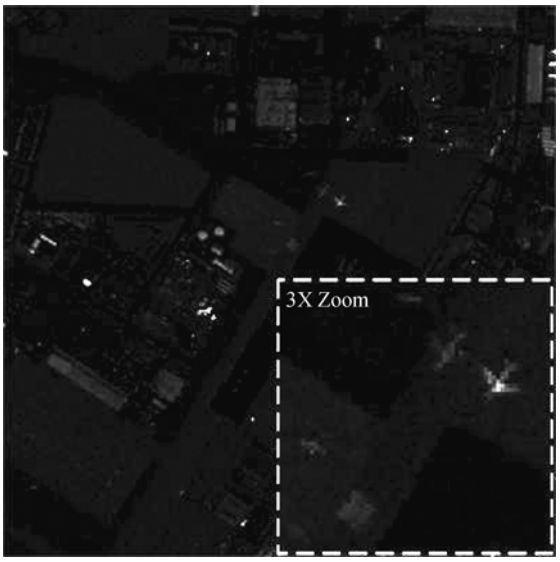

图 2 RXD-UDT 异常探测结果

对原反射率图像采用邻域光谱度量指数以及邻域独立端元指数进行空间维信息的提取(本文以Sobel 算子与拉普拉斯算子为例对目标提取效果进行评价), 图 3 和图 4 分别列举了提取的结果。

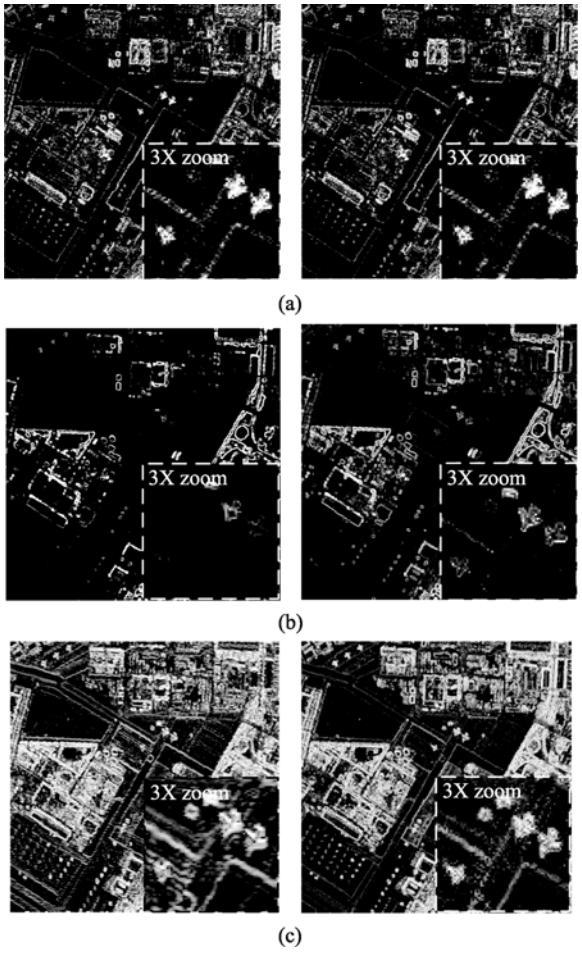

图 3 邻域光谱度量指数结果
(a) *SDM* (*MD*); (b) *SAM*; (c) *SID*
(左侧: Sobel 算子; 右侧: 拉普拉斯算子)

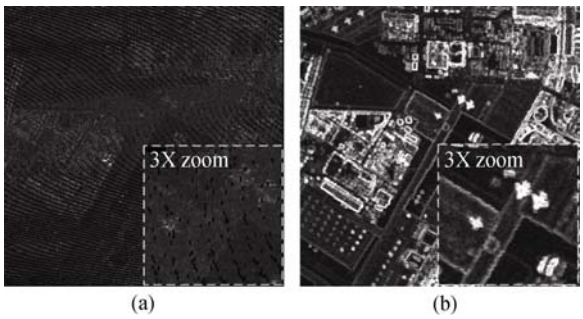

图 4 邻域独立端元指数结果
(a) *EBDI*; (b) *CDI*

在邻域光谱度量指数中, Sobel 算子与拉普拉斯算子两者在*SDM*的比较中发现, Sobel算子对线状轮廓提取较为清晰, 但对房屋、飞机等不规则形状地物的轮廓的提取却不如拉普拉斯算子; 在 *SAM* 中, 两者所提取的轮廓比其他指数要细(例如右下角放大的飞机边缘轮廓清晰可见), 但同时也丢失了跑道、平地、房屋的轮廓, 并且在图中明显发现, 采用 Sobel 算子所丢失的线状细节比拉普拉斯算子要多; 在 *SID* 中, 两者所提取的轮廓都较清晰, 尤其对于相对较小的目标(如图像中放大的飞机、图像左下角平地内多个整齐排列的小目标), 能清晰地区分出来, 但两个结果图中均存在一定的噪声, 尤其是 Sobel 算子的结果中, 左上方均匀地块中噪声的干扰较为明显。

在邻域独立端元指数的结果中发现, *CDI* 能够较好地提取出平地、跑道、房屋、飞机的轮廓, 尤其是飞机目标能够清晰可见。但 *EBDI* 未能有效地提取图像的细节信息, 其原因是地物存在着一定的连续性, 中心像元的光谱信号很容易淹没在周围某些相似像元光谱所张的子空间当中。尽管 *CDI* 也通过端元与子空间的距离得到, 但该指数计算的是各像元最大投影距离的累计值, 因此单个或部分相似像元光谱不足以影响整个累计距离。可见, *CDI* 有效避免了邻域内相似像元光谱的影响。

5 结论与讨论

本文探讨了两类邻域指数: 邻域光谱度量指数和邻域独立端元指数。

在邻域光谱度量指数中, *SDM* 有利于对线状(如机场跑道)轮廓的提取, 但对于点状地物这类小目标的效果不如 *SID* 以及 *CDI*; *SAM* 所提取的轮廓较细, 但对线状、较大的面状地物(如跑道、操场), 不建议使用 *SAM* 进行提取; *SID* 能较好地提取点状小目标, 对线状轮廓的提取效果也较好, 但 *SID* 受噪声的影响较大, 当图像存在较大的噪声时, 使用该指数前, 建议先进行有效的去噪预处理。

在邻域独立端元指数中, *EBDI* 容易受邻近相似地物光谱的干扰, 因此, 对于具有空间连续性的地物, 包括线状、面状连续性以及辐射能量的影响范围超过一个像元的目标, 均不建议采用该指数进行提取; *CDI* 对于飞机、点状地物等小目标具有较强的提取能力, 线状(如跑道)、较大面积的块状(如操场)以及结构较复杂的地物(如各种形状的房屋)的提取效果也较好, 因此, 该指数具有较好的适应性, 可应用于对各种地物的提取。

对本文所提出的各种邻域指数进行空间分辨率级别的检验; 考虑更多合理的光谱度量空间函数进行实验验证, 并发展新的、有效的邻域指数; 结合目

标地物几何特征与光谱特征进行高精度目标探测与识别是下一步工作的重点。

致 谢 感谢 JPL (Jet Propulsion Laboratory)以及 ENVI (The Environment for Visualizing Images, ITT 版权所有)提供的 AVIRIS 实验数据。

REFERENCES

Bakker W H and Schmidt K S. 2002. Hyperspectral edge filtering for measuring homogeneity of surface cover types. *Journal of Photogrammetry & Remote Sensing*, 2002, **56**: 246—256

Bourbaki N. 1987. Topological Vector Spaces, Chapters 1—5: Elements of Mathematics. Berlin: Springer-Verlag

Chang C I. 2002. Hyperspectral Imageing Techniques for Spectral Detection and Classification. New York: Kluwer Academic/ Plenum Publishers

Chang C I. 2000. An information theoretic-based approach to spectral variability, similarity and discriminability for hyperspectral image analysis. *IEEE Transation on Information Theory*, **46**(5): 1927—1932

Du Y, Chang C I, Ren H, Amico F D and Jensen J O. 2003. A new hyperspectral discrimination measure for spectral similarity. Algorithms and Technologies for Multispectral, Hyperspectral, and Ultraspectral Imagery IX, SPIE Digital Library

Gong Y and Bi D. 2007. The edge detection of hyperspectral image based on its proportion image. 27th International Congress on High-Speed Photography and Photonics. SPIE Digital Library

Kanade T and Shafer S. 1987. Image understanding research at cmu. Proceedings of an Image Understanding Workshop, Los Angeles, CA:Morgan Kaufmann Publishers

Kenneth R C. 2002. Digital Image Processing 2ed. Beijing: Publishing House of Electronics Industry

Luo W F, Zhong L, Zhang B and Gao L R. 2008. An spectral unmixing algorithm for hyperspectral image based on the distance to subspace. *Progress in Natural Science*, **18**(10):1175—1180

Schowengerdt R A. 2006. Remote Sensing 3ed: Models and Methods for Image Processing. Missouri, USA :Academic Press

Tong Q X, Zhang B and Zheng L F. 2006. Hyperspectral Remote Sensing. Beijing: Higher Education Press

Verzakov S, Paclik P and Duin R P W. 2006. Edge detection in hyperspectral imaging: multivariate statistical approaches. Lecture Notes in Computer Science. Berlin:Springer Verlag

附中文参考文献

罗文斐, 钟亮, 张兵, 高连如. 2008. 基于子空间距离的高光谱图像光谱解混算法. 自然科学进展, **18**(10): 1175—1180

童庆禧, 张兵, 郑兰芬. 2006. 高光谱遥感: 原理、技术与应用. 北京: 高等教育出版社